Enhanced Electron-Spin Coherence in a GaAs Quantum Emitter

Giang N. Nguyen,[1,*] Clemens Spinnler,[1] Mark R. Hogg,[1] Liang Zhai,[1] Alisa Javadi,[1,†] Carolin A. Schrader,[1] Marcel Erbe,[1] Marcus Wyss,[2] Julian Ritzmann,[3] Hans-Georg Babin,[3] Andreas D. Wieck,[3] Arne Ludwig,[3] and Richard J. Warburton[1]

[1]*Department of Physics, University of Basel, 4056 Basel, Switzerland*

[2]*Swiss Nanoscience Institute, University of Basel, 4056 Basel, Switzerland*

[3]*Lehrstuhl für Angewandte Festkörperphysik, Ruhr-Universität Bochum, 44780 Bochum, Germany*

(Received 5 July 2023; accepted 18 October 2023; published 22 November 2023)

A spin-photon interface should operate with both coherent photons and a coherent spin to enable cluster-state generation and entanglement distribution. In high-quality devices, self-assembled GaAs quantum dots are near-perfect emitters of on-demand coherent photons. However, the spin rapidly decoheres via the magnetic noise arising from the host nuclei. Here, we address this drawback by implementing an all-optical nuclear-spin cooling scheme on a GaAs quantum dot. The electron-spin coherence time increases 156-fold from $T_2^* = 3.9$ ns to 0.608 μs. The cooling scheme depends on a non-collinear term in the hyperfine interaction. The results show that such a term is present even though the strain is low and no external stress is applied. Our work highlights the potential of optically active GaAs quantum dots as fast, highly coherent spin-photon interfaces.

DOI: 10.1103/PhysRevLett.131.210805

Photonic quantum technologies require quantum emitters capable of high-fidelity and high-rate operation. Of particular interest for quantum networks [1–6] and measurement-based quantum computing [7–9] are platforms that host a spin [10–12], allowing the creation of spin-photon interfaces.

Self-assembled semiconductor quantum dots (QDs) are potential candidates for spin-photon interfaces due to the deterministic photon emission at exceptionally high quality and rates [13–16] and the ability to load a QD with a single electron or hole [17]. This has led to demonstrations of spin-photon entanglement [18–21], distant spin-spin entanglement [22,23], and the creation of multiphoton cluster states [24–26]. However, in these previous experiments, the short spin coherence times, $T_2^* \sim 1$–10 ns, limited the entanglement fidelity. The short T_2^* is a consequence of magnetic noise in the host nuclear spins, coupling to the electron spin via the hyperfine interaction [27–29].

A powerful way to mitigate the short T_2^* is to cool the nuclear spins to ultralow temperatures in order to reduce the fluctuations. The nuclei can be cooled via the electron spin itself, exploiting the hyperfine interaction [30]. In an optical experiment, this was originally demonstrated on an ensemble of QDs [31]. On single QDs, nuclear-spin cooling was demonstrated on gate-defined GaAs QDs via a measure-and-correct feedback loop [32,33]. More recently, the highly inhomogeneous nuclear spins of a self-assembled InGaAs QD were cooled via an autonomous feedback [34]. Subsequently, a quantum sensing protocol was employed, narrowing the nuclear distribution further, thereby increasing T_2^* to 300 ns [35]. For both schemes, a noncollinear term in the hyperfine interaction is required to allow for the cooling of the nuclei. In contrast to the collinear term from the contact hyperfine interaction ($\propto S_z I_z$), the noncollinear term ($\propto S_z I_x$) arises from nuclear quadrupolar fields in strained QDs; here S_z (I_z) is the electron (nuclear) spin operator along the direction of the applied magnetic field [30,36,37].

The most studied QDs for spin-photon applications are QDs in the InGaAs/GaAs system. InGaAs QDs are self-assembled via the strain-driven Stanski-Krastanov mechanism. GaAs QDs in an AlGaAs matrix represent an alternative platform. The strain is low such that these QDs are self-assembled via an alternative mechanism, droplet-etching. Low-noise GaAs QDs have excellent photonic properties, all at a convenient wavelength (around 780 nm). In high-quality material, the optical linewidths are within 10% of the transform limit [38]. Photons emitted by remote QDs have achieved a two-photon interference visibility of 93% without spectral or temporal filtering [39]. The biexciton cascade generates entangled photon pairs with an extremely high entanglement concurrence [40]. In terms of the nuclear spins, the lack of both strain and spin-$\frac{9}{2}$ In atoms results in a homogeneous nuclear-spin ensemble [41], as demonstrated by the success of the Carr-Purcell-Meiboom-Gill (CPMG) decoupling scheme in prolonging the electron-spin T_2 from 3.8 to 113 μs [42]. However, as for InGaAs QDs, noise in the nuclear-spin limits T_2^* to values of a few ns. To date, the possibility of feedback cooling the nuclear spins via the electron spin has remained uncertain, due to the predicted absence of the strain-generated noncollinear hyperfine interaction.

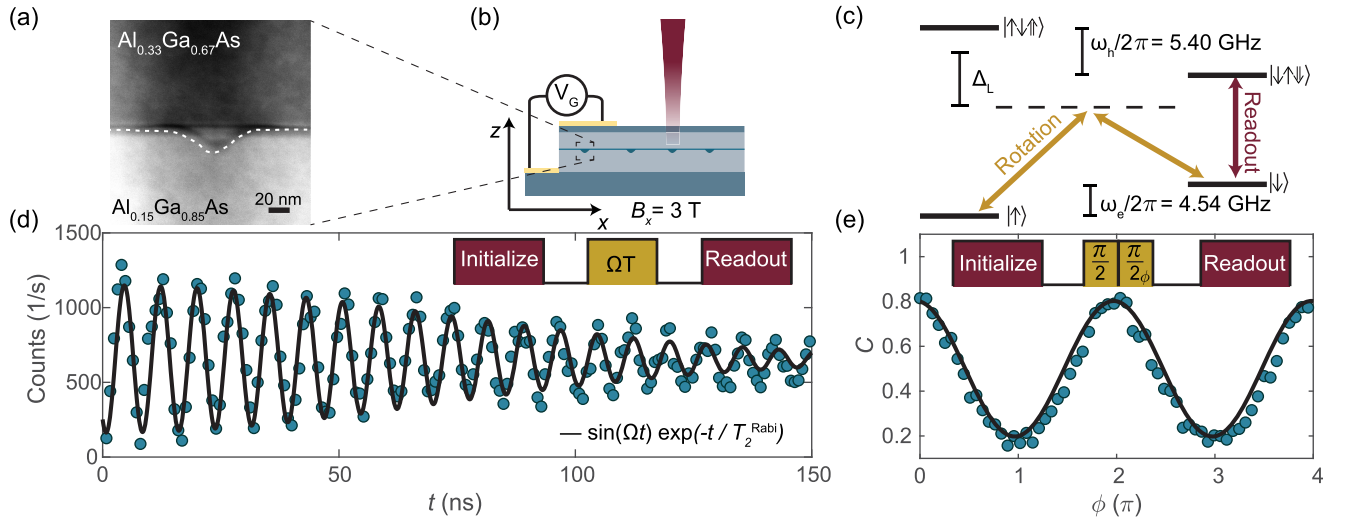

FIG. 1. Coherent spin control of an electron in a droplet-etched GaAs QD. (a) High-angle dark-field scanning transmission image of a droplet-etched GaAs QD. The dashed line is a guide to the eye to describe the droplet shape. (b) Schematic of the sample design: a layer of GaAs QDs is embedded in a diode structure. A magnetic field perpendicular to the growth direction defines the quantization axis. (c) Energy level diagram of a charged QD in an in-plane magnetic field. The "vertical" transitions are x polarized while the "diagonal" transitions are y polarized. A circularly polarized rotation pulse detuned by $\Delta_L = 700$ GHz drives a Raman transition between the electron-spin states. The readout laser is on resonance with the lower-frequency (vertical) transition and initializes the electron into the $|\uparrow\rangle$ state. (d) Electron-spin Rabi oscillations as a function of drive time t. The solid line is an exponential fit to the data with $T_2^{\mathrm{Rabi}} = 73(5)$ ns. (e) Full control of the rotation axis about the Bloch sphere using two consecutive $(\pi/2)$ pulses as a function of the phase ϕ of the second pulse. The solid line is a sinusoidal fit to the data.

Here, we implement all-optical cooling schemes on low-noise GaAs QDs and demonstrate an increase in the electron-spin coherence time from $T_2^* = 3.9$ ns to 0.608 μs. This is achieved with autonomous feedback and without any external perturbation (such as strain tuning). We demonstrate spin control with $T_2^* = 0.608$ μs, an extension of T_2 with CPMG (with a scaling of $T_2^{\mathrm{CPMG}} \propto N^{0.69}$ matching previous experiments [42]), fast spin rotations (Rabi frequencies above 100 MHz), and high-fidelity spin control ($F_\pi > 98\%$). Our results establish GaAs QDs as an emitter of coherent photons and a host to a coherent spin.

To create the QDs, droplet-etched nanoholes in an $Al_{0.15}Ga_{0.85}As$ matrix are filled with GaAs and capped by an $Al_{0.33}Ga_{0.67}As$ layer. The materials are almost lattice-matched. Figure 1(a) shows a high-angle dark-field scanning transmission (HAADF-STEM) image of a GaAs QD [43]. Notable is a thin, Al-rich layer at the bottom surface of the QD [43]. The QD is embedded in a p-i-n diode structure [see Fig. 1(b)] such that the QD charge is stabilized via the Coulomb blockade. Individual QDs exhibit near-transform-limited optical linewidths [38,39,43]. A 3.00 T magnetic field is applied perpendicular to the growth direction (Voigt geometry), at an angle of 45° to the in-plane crystal axes. The electron Zeeman frequency is $f_Z = 4.54$ GHz corresponding to a g factor of $g_e = -0.11$.

The spin is manipulated by a two-color Raman pulse detuned from the excited states by $\Delta_L = 700$ GHz [see Fig. 1(c)]. This pulse is created by amplitude-modulating circularly polarized light with an electro-optic modulator driven by an arbitrary waveform generator [43,55]. A laser resonant with the red "vertical" transition is used to read out the spin (such that the $|\downarrow\rangle$ state is bright, the $|\uparrow\rangle$ state is dark) and to prepare the spin in the $|\uparrow\rangle$ state via optical spin pumping [43].

Driving the electron-spin resonance (ESR) [Fig. 1(d)] shows clear Rabi oscillations between $|\uparrow\rangle$ and $|\downarrow\rangle$ with increasing drive time t. We find an exponential decay of the oscillations with $T_2^{\mathrm{Rabi}} = 73(5)$ ns, corresponding to a quality factor of $Q = 2T_2^{\mathrm{Rabi}} f_{\mathrm{Rabi}} = 19(1)$ and π-pulse fidelity $f_\pi = \frac{1}{2}(1 + e^{-1/Q}) = 0.975(2)$ at $\Omega = 2\pi \times 130$ MHz. As has been observed for InGaAs QDs [55], we find a strong modulation of the quality factor [43] when the electron spin is driven close to the nuclear Larmor frequencies ω_n (i.e., $\Omega \sim \omega_n$), a signature of an electron-nuclei interaction via a Hartmann-Hahn resonance [56].

We access rotation around a second axis on the Bloch sphere by controlling the phase of the microwave signal that is imprinted on the optical field. Figure 1(e) shows the sinusoidal response after two consecutive $(\pi/2)$ pulses on changing the phase ϕ of the second pulse, thereby demonstrating rotation around an arbitrary axis on the equator of the Bloch sphere.

On driving Rabi oscillations as a function of the detuning Δ with respect to the Zeeman frequency ($\Delta = f_Z - f_{\mathrm{probe}}$), we find strong deviations from the typical chevron pattern

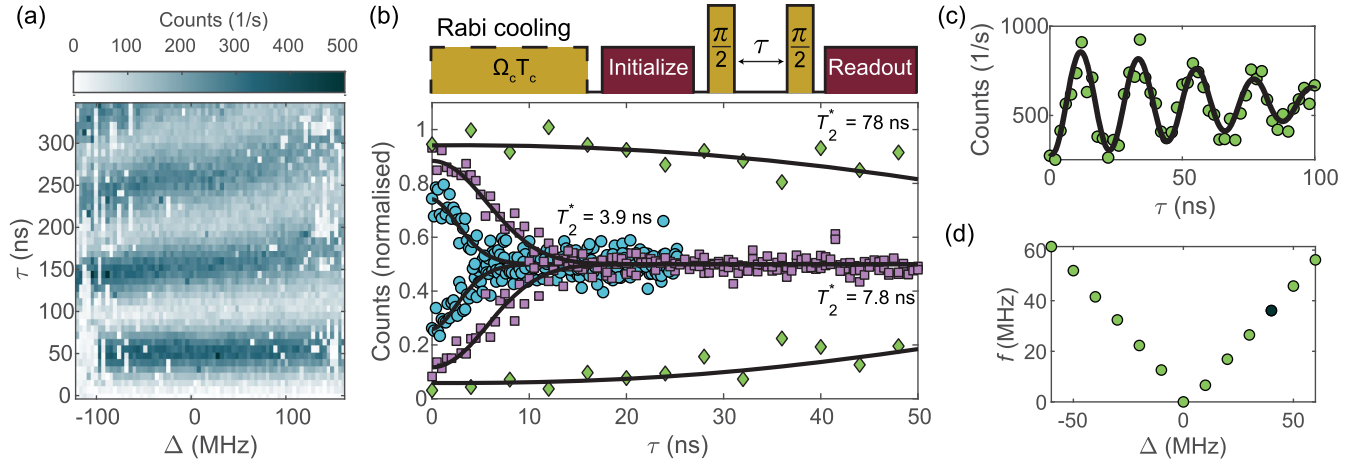

FIG. 2. Locking of electron-spin resonance (ESR) and cooling of nuclei with a Rabi drive. (a) Rabi oscillations versus detuning show locking of the ESR to the drive within a window of frequencies and unstable Rabi oscillations outside the window. (b) Top: Pulse sequence for Ramsey interferometry with prior Rabi cooling. For Rabi cooling a $T_c = 1$ μs long pulse at a Rabi frequency of $\Omega_c = 2\pi \times 17$ MHz is used. The Ramsey experiment was performed at a larger Rabi frequency of $2\pi \times 100$ MHz. Bottom: Top and bottom envelopes of the Ramsey interferometry with 100 μs pause (circles), zero pause (squares), and Rabi cooling (diamonds); the extracted coherence times are $T_2^* = 3.9(2)$, $T_2^* = 7.8(2)$, and $T_2^* = 78(2)$ ns, respectively. Counts are normalized to 0.5 for long delays. (c) Ramsey interferometry at a probe detuning with respect to the cooling frequency of $\Delta = 40$ MHz [black dot in (d)]. (d) Oscillation frequency f in Ramsey interferometry as a function of detuning of probe and cooling frequency Δ. The solid lines in (b) and (c) are Gaussian fits to the data.

expected for a two-level system [see Fig. 2(a)]. In a ∼200 MHz window around the Zeeman frequency, we find that the spin rotations lock to the probe frequency f_{probe}, a clear signature of electron-spin–nuclear-spin coupling [37,57–59].

When the ESR is locked via the hyperfine interaction, cooling of the nuclei, equivalently narrowing of the nuclear distribution, is predicted [60,61]. This can be quantified by a reduction in σ_{OH}, the standard deviation of the ESR frequency fluctuations due to the changing Overhauser field. To probe this, we perform a free-induction decay (FID) experiment to measure the electron coherence time T_2^* in a Ramsey experiment, which acts as a gauge of the temperature of the nuclear-spin ensemble ($\sigma_{\text{OH}} \propto T_2^*$) [28,29]. We compare the bare T_2^* to that obtained after locking the ESR [see Fig. 2(b)]. We observe a 20-fold increase from $T_2^* = 3.9(2)$ to 78(2) ns corresponding to a narrowing of σ_{OH} from 52(1) to 2.90(5) MHz following the Rabi drive. Remarkably, we already find an enhancement in coherence time without a dedicated cooling pulse when the Ramsey experiment is carried out with a high duty cycle: repetitive Ramsey experiments lead to a T_2^* of 7.8(2) ns. To determine the bare electron coherence time, we add a 100 μs buffer between each cycle. This observation suggests that the repetitive application of spin manipulation pulses as short as 4 ns already leads to a narrowing of σ_{OH}.

We confirm the nuclear-spin cooling and locking of the ESR to the Rabi drive by fixing the cooling frequency f_c during Rabi cooling, subsequently detuning the probe frequency f_{probe} in a Ramsey experiment. As expected for a classic Ramsey experiment, oscillations arise at the detuning frequencies $\Delta = f_c - f_{\text{probe}}$ [see Figs. 2(c) and 2(d)], now with an increased coherence time.

To cool the nuclei further, we implement the recently developed quantum-sensing-based cooling scheme [35]. In this protocol, each cooling cycle consists of three steps [see Fig. 3(a), top]: (i) The electron spin is initialized and then rotated to the equator with a $(\pi/2)$ pulse. A period of free evolution τ_{sense} allows the electron to sense the Overhauser field fluctuation that leads to a detuning Δ from the target frequency f_c. (ii) A coherent electron-nuclei flip-flop interaction arising from a noncollinear term in the hyperfine interaction is activated through ESR driving at Hartmann-Hahn resonance $\Omega \approx \omega_n$. The sign of the detuning Δ determines the direction of the nuclear flops and thus leads to a reversal of the measured fluctuation. (iii) A projective measurement of the spin state transfers entropy from the nuclei and concludes one cycle of the cooling scheme. Repeating this cycle with increasing sensing time τ results in a narrower feedback function in each cycle and hence an increased sensitivity to changes in σ_{OH}.

We find optimal parameters for the quantum-sensing-based cooling at $N = 40$ cycles with a linearly increasing sensing time τ_{sense} from $\tau_{\text{min}} = 20$ to $\tau_{\text{max}} = 400$ ns, and electron-nuclei drive time $T_c = 125$ ns at a Rabi frequency $\Omega_c = 2\pi \times 17$ MHz, followed by a spin pumping pulse of 200 ns [43]. This preparation sequence takes ∼22 μs and is repeated before each Ramsey cycle.

The electron coherence time T_2^* increases from 3.9(2) ns to 0.608(13) μs after application of the protocol [see Figs. 3(a) and 3(b)]. This constitutes a 156-fold increase in T_2^*. The final T_2^* is a factor of 2 larger than the previous

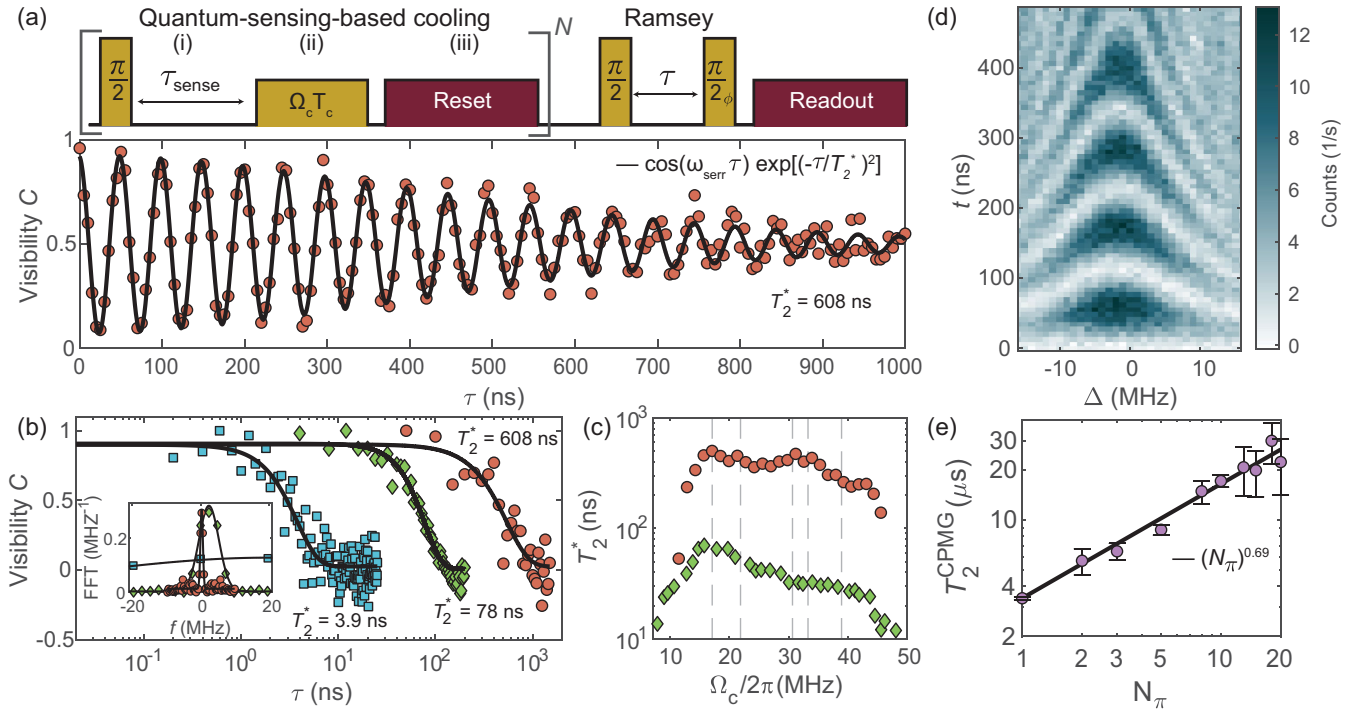

FIG. 3. Quantum-sensing-based cooling and dynamical decoupling. (a) Top: Pulse scheme for the quantum-sensing-based cooling consisting of (i) a sensing step, (ii) a driven electron-nuclei interaction, and (iii) a reset. The last reset pulse in the cooling scheme initializes the electron spin for the Ramsey experiment performed at a Rabi frequency of $2\pi \times 100$ MHz. Bottom: Ramsey interferometry with serrodyne frequency $\omega_{\mathrm{serr}} = 2\pi \times 20$ MHz [$\phi(\tau) = \sin(\omega_{\mathrm{serr}}\tau)$] following quantum-sensing-based cooling gives $T_2^* = 0.608(13)$ μs. (b) Comparison of T_2^* before cooling (squares), after Rabi cooling (diamonds), and after quantum-sensing-based cooling (circles). Inset: fast Fourier transform of the Ramsey visibilities gives $\sigma_{\mathrm{OH}} = 52(1)$, $\sigma_{\mathrm{OH}} = 2.90(5)$, and $\sigma_{\mathrm{OH}} = 0.355(4)$ MHz, respectively. (c) T_2^* versus Rabi frequency during cooling (Ω_c) for Rabi cooling (diamonds) and quantum-sensing-based cooling (circles). Dashed lines correspond to nuclear Larmor frequencies, from left to right: $\Delta\omega = 2\pi \times 17.08$, $\omega(^{75}\mathrm{As}) = 2\pi \times 21.9$, $\omega(^{69}\mathrm{Ga}) = 2\pi \times 30.7$, $\omega(^{27}\mathrm{Al}) = 2\pi \times 33.28$, and $\omega(^{71}\mathrm{Ga}) = 2\pi \times 39.0$ MHz. (d) Rabi oscillations at $\Omega = 2\pi \times 8.9$ MHz as a function of detuning from f_c following quantum-sensing-based cooling. (e) Dynamical decoupling of the electron spin with a CPMG sequence. The solid lines in (a),(b) are Gaussian fits to the data. The solid line in (e) is a power law fit to the data.

highest T_2^* reported on an electron spin hosted by an InGaAs QD (296 ns [35]) and just below the highest reported T_2^* of a single electron-spin qubit in a gate-defined GaAs QD (767 ns [33]). The enhancement corresponds to a narrowing of the nuclear-spin ensemble from $\sigma_{\mathrm{OH}} = 52(1)$ to 0.355(4) MHz [see Fig. 3(b), inset].

Using hyperfine constants A_k and abundancies η_k of the nuclei species $k \in \{^{69}\mathrm{Ga}, ^{71}\mathrm{Ga}, ^{75}\mathrm{As}\}$ we can estimate the number of nuclei involved $N = 5/4 \sum_k \eta_k A_k^2 T_2^{*2} = 1.4 \times 10^5$ and estimate the hyperfine interaction per nuclei $A_c = 1/(\sqrt{5N/2}\pi T_2^*) = 0.13$ MHz [27,35,42]. This corresponds to a distribution of $\sigma_{\mathrm{OH}}/A_c \approx 376.8$ macrostates in the uncooled state and 2.6 after quantum-sensing-based cooling, entering the regime where just a few nuclei excitations remain.

For both the quantum-sensing-based and Rabi cooling schemes, the Rabi frequency Ω_c is an important parameter [see Fig. 3(c)]. The maximum performance for both cooling schemes occurs at $\Omega_c = 2\pi \times 17$ MHz, close to the difference frequency of ^{71}Ga and ^{75}As [$\Delta\omega = \omega(^{71}\mathrm{Ga}) - \omega(^{75}\mathrm{As}) = 2\pi \times 17.08$ MHz]. This result is in contrast to those on InGaAs QDs for which cooling was most effective at a direct Hartmann-Hahn resonance [35]. Generally speaking, the fact that cooling via an autonomous feedback process is effective on GaAs QDs shows that a noncollinear term in the hyperfine interaction [30,37,57] must be present even though the strain in the QDs is small.

Following cooling, a typical chevron pattern is observed on driving Rabi oscillations as a function of detuning with respect to the cooling frequency f_c [Fig. 3(d)], using here a Rabi frequency below the Hartmann-Hahn resonances. This demonstrates that in this case the electron spin is isolated from the nuclear environment and behaves as a two-level system. In addition, the quality factor of the oscillations now increases to $Q = 30.0(14)$ [corresponding to a π-pulse fidelity of 98.4(1)%] [43], consistent with a reduction of hyperfine-interaction-induced Rabi decay.

Recent experiments showed that the electron-spin T_2 can be increased by implementing a decoupling scheme, the CPMG protocol. As a final step, we verify that this is also

possible on the QD for which nuclear-spin cooling was highly effective [see Fig. 3(d)]. By applying CPMG pulses, we extend T_2 from $T_2^{\mathrm{HE}} = 2.93(6)$ μs using a Hahn echo ($N_\pi = 1$) to $T_2^{\mathrm{CPMG}} = 22(8)$ μs, an order of magnitude increase, with $N_\pi = 20$ pulses. We extract a T_2 scaling of $T_2^{\mathrm{CPMG}} \propto N_\pi^\gamma$ with $\gamma = 0.69(12)$, consistent with recent results on droplet-etched QDs [42] and gate-defined QDs [62]. This result confirms that the nuclear-spin ensemble is highly homogeneous. The application of more pulses is currently limited by imperfect pulse calibrations and the electron-spin relaxation time $T_1 \sim 40$ μs [43].

In conclusion, we have demonstrated fast and flexible optical control of an electron spin confined to a self-assembled GaAs QD. We show that autonomous feedback protocols to cool the nuclear spins are very effective even on an as-grown, close-to-strain-free QD. Nuclear-spin cooling leads to a 156-fold increase in the T_2^* time, $T_2^* = 0.608$ μs. Furthermore, both T_2^* and T_2 can be extended on exactly the same QD, T_2^* by nuclear-spin cooling, T_2 by dynamic decoupling. These results imply that a small noncollinear term must be present in the hyperfine Hamiltonian. Following nuclear-spin cooling, T_2^* is still far from T_2, suggesting that more advanced cooling techniques are necessary to fully remove the inhomogeneous broadening [63]. Nonetheless, T_2^* becomes much longer than both the time required to rotate the spin and the time required to generate a photon. Together with recent results on the generation of indistinguishable photons from remote GaAs QDs [39] performed on the same sample as used in this experiment, our results highlight the promise of GaAs QDs for a coherent spin-photon interface.

We thank Ming-Lai Chan and Peter Lodahl at the Niels-Bohr Institute, Leon Zaporski and Mete Atatüre at the University of Cambridge, and Dorian Gangloff at the University of Oxford for stimulating discussions. The work was supported by SNF Project 200020_204069 and Horizon 2020 FET-Open Project QLUSTER. G. N. N., M. E., L. Z., and A. J. received funding from the European Union's Horizon 2020 Research and Innovation Programme under the Marie Skłodowska-Curie Grant Agreement No. 861097 (QUDOT-TECH), No. 721394 (4PHOTON), and No. 840453 (HiFig), respectively. H. G. B., J. R., A. D. W., and A. L. acknowledge financial support from the Grants DFH/UFA CDFA05-06, DFG TRR160, DFG project 383065199, and BMBF Q.Link.X 16KIS0867.

*giang.nguyen@unibas.ch
†Present address: School of Electrical and Computer Engineering, University of Oklahoma, Norman, Oklahoma 73019, USA.

[1] S. Wehner, D. Elkouss, and R. Hanson, Quantum internet: A vision for the road ahead, Science **362**, 9288 (2018).
[2] M. Pompili, S. L. N. Hermans, S. Baier, H. K. C. Beukers, P. C. Humphreys, R. N. Schouten, R. F. L. Vermeulen, M. J. Tiggelman, L. dos Santos Martins, B. Dirkse, S. Wehner, and R. Hanson, Realization of a multinode quantum network of remote solid-state qubits, Science **372**, 259 (2021).
[3] P.-J. Stas, Y. Q. Huan, B. Machielse, E. N. Knall, A. Suleymanzade, B. Pingault, M. Sutula, S. W. Ding, C. M. Knaut, D. R. Assumpcao, Y.-C. Wei, M. K. Bhaskar, R. Riedinger, D. D. Sukachev, H. Park, M. Lončar, D. S. Levonian, and M. D. Lukin, Robust multi-qubit quantum network node with integrated error detection, Science **378**, 557 (2022).
[4] K. Azuma, K. Tamaki, and H.-K. Lo, All-photonic quantum repeaters, Nat. Commun. **6**, 6787 (2015).
[5] D. Buterakos, E. Barnes, and S. E. Economou, Deterministic Generation of All-Photonic Quantum Repeaters from Solid-State Emitters, Phys. Rev. X **7**, 041023 (2017).
[6] J. Borregaard, H. Pichler, T. Schröder, M. D. Lukin, P. Lodahl, and A. S. Sørensen, One-Way Quantum Repeater Based on Near-Deterministic Photon-Emitter Interfaces, Phys. Rev. X **10**, 021071 (2020).
[7] R. Raussendorf and H. J. Briegel, A one-way quantum computer, Phys. Rev. Lett. **86**, 5188 (2001).
[8] D. E. Browne and T. Rudolph, Resource-efficient linear optical quantum computation, Phys. Rev. Lett. **95**, 010501 (2005).
[9] M. Gimeno-Segovia, P. Shadbolt, D. E. Browne, and T. Rudolph, From three-photon Greenberger-Horne-Zeilinger states to ballistic universal quantum computation, Phys. Rev. Lett. **115**, 020502 (2015).
[10] M. Atatüre, D. Englund, N. Vamivakas, S.-Y. Lee, and J. Wrachtrup, Material platforms for spin-based photonic quantum technologies, Nat. Rev. Mater. **3**, 38 (2018).
[11] A. Laucht *et al.*, Roadmap on quantum nanotechnologies, Nanotechnology **32**, 162003 (2021).
[12] T. Fujita, K. Morimoto, H. Kiyama, G. Allison, M. Larsson, A. Ludwig, S. R. Valentin, A. D. Wieck, A. Oiwa, and S. Tarucha, Angular momentum transfer from photon polarization to an electron spin in a gate-defined quantum dot, Nat. Commun. **10**, 2991 (2019).
[13] N. Somaschi, V. Giesz, L. De Santis, J. C. Loredo, M. P. Almeida, G. Hornecker, S. L. Portalupi, T. Grange, C. Antón, J. Demory, C. Gómez, I. Sagnes, N. D. Lanzillotti-Kimura, A. Lemaítre, A. Auffeves, A. G. White, L. Lanco, and P. Senellart, Near-optimal single-photon sources in the solid state, Nat. Photonics **10**, 340 (2016).
[14] H. Wang *et al.*, Towards optimal single-photon sources from polarized microcavities, Nat. Photonics **13**, 770 (2019).
[15] R. Uppu, F. T. Pedersen, Y. Wang, C. T. Olesen, C. Papon, X. Zhou, L. Midolo, S. Scholz, A. D. Wieck, A. Ludwig, and P. Lodahl, Scalable integrated single-photon source, Sci. Adv. **6**, eabc8268 (2020).
[16] N. Tomm, A. Javadi, N. O. Antoniadis, D. Najer, M. C. Löbl, A. R. Korsch, R. Schott, S. R. Valentin, A. D. Wieck, A. Ludwig, and R. J. Warburton, A bright and fast source of coherent single photons, Nat. Nanotechnol. **16**, 399 (2021).
[17] R. J. Warburton, Single spins in self-assembled quantum dots, Nat. Mater. **12**, 483 (2013).
[18] K. De Greve, L. Yu, P. L. McMahon, J. S. Pelc, C. M. Natarajan, N. Y. Kim, E. Abe, S. Maier, C. Schneider,

M. Kamp, S. Höfling, R. H. Hadfield, A. Forchel, M. M. Fejer, and Y. Yamamoto, Quantum-dot spin–photon entanglement via frequency downconversion to telecom wavelength, Nature (London) **491**, 421 (2012).

[19] W. B. Gao, P. Fallahi, E. Togan, J. Miguel-Sanchez, and A. Imamoglu, Observation of entanglement between a quantum dot spin and a single photon, Nature (London) **491**, 426 (2012).

[20] J. R. Schaibley, A. P. Burgers, G. A. McCracken, L.-M. Duan, P. R. Berman, D. G. Steel, A. S. Bracker, D. Gammon, and L. J. Sham, Demonstration of quantum entanglement between a single electron spin confined to an InAs quantum dot and a photon, Phys. Rev. Lett. **110**, 167401 (2013).

[21] M. H. Appel, A. Tiranov, S. Pabst, M. L. Chan, C. Starup, Y. Wang, L. Midolo, K. Tiurev, S. Scholz, A. D. Wieck, A. Ludwig, A. S. Sørensen, and P. Lodahl, Entangling a Hole spin with a time-bin photon: A waveguide approach for quantum dot sources of multiphoton entanglement, Phys. Rev. Lett. **128**, 233602 (2022).

[22] A. Delteil, Z. Sun, W.-b. Gao, E. Togan, S. Faelt, and A. Imamoğlu, Generation of heralded entanglement between distant hole spins, Nat. Phys. **12**, 218 (2016).

[23] R. Stockill, M. J. Stanley, L. Huthmacher, E. Clarke, M. Hugues, A. J. Miller, C. Matthiesen, C. Le Gall, and M. Atatüre, Phase-tuned entangled state generation between distant spin qubits, Phys. Rev. Lett. **119**, 010503 (2017).

[24] I. Schwartz, D. Cogan, E. R. Schmidgall, Y. Don, L. Gantz, O. Kenneth, N. H. Lindner, and D. Gershoni, Deterministic generation of a cluster state of entangled photons, Science **354**, 434 (2016).

[25] D. Cogan, Z.-E. Su, O. Kenneth, and D. Gershoni, Deterministic generation of indistinguishable photons in a cluster state, Nat. Photonics **17**, 324 (2023).

[26] N. Coste, D. A. Fioretto, N. Belabas, S. C. Wein, P. Hilaire, R. Frantzeskakis, M. Gundin, B. Goes, N. Somaschi, M. Morassi, A. Lemaître, I. Sagnes, A. Harouri, S. E. Economou, A. Auffeves, O. Krebs, L. Lanco, and P. Senellart, High-rate entanglement between a semiconductor spin and indistinguishable photons, Nat. Photonics **17**, 582 (2023).

[27] I. A. Merkulov, Al. L. Efros, and M. Rosen, Electron spin relaxation by nuclei in semiconductor quantum dots, Phys. Rev. B **65**, 205309 (2002).

[28] Ł. Cywiński, W. M. Witzel, and S. Das Sarma, Pure quantum dephasing of a solid-state electron spin qubit in a large nuclear spin bath coupled by long-range hyperfine-mediated interactions, Phys. Rev. B **79**, 245314 (2009).

[29] W. A. Coish and D. Loss, Hyperfine interaction in a quantum dot: Non-Markovian electron spin dynamics, Phys. Rev. B **70**, 195340 (2004).

[30] W. Yang and L. J. Sham, General theory of feedback control of a nuclear spin ensemble in quantum dots, Phys. Rev. B **88**, 235304 (2013).

[31] A. Greilich, A. Shabaev, D. R. Yakovlev, Al. L. Efros, I. A. Yugova, D. Reuter, A. D. Wieck, and M. Bayer, Nuclei-induced frequency focusing of electron spin coherence, Science **317**, 1896 (2007).

[32] M. D. Shulman, S. P. Harvey, J. M. Nichol, S. D. Bartlett, A. C. Doherty, V. Umansky, and A. Yacoby, Suppressing qubit dephasing using real-time Hamiltonian estimation, Nat. Commun. **5**, 5156 (2014).

[33] T. Nakajima, A. Noiri, K. Kawasaki, J. Yoneda, P. Stano, S. Amaha, T. Otsuka, K. Takeda, M. R. Delbecq, G. Allison, A. Ludwig, A. D. Wieck, D. Loss, and S. Tarucha, Coherence of a Driven Electron Spin Qubit Actively Decoupled from Quasistatic Noise, Phys. Rev. X **10**, 011060 (2020).

[34] D. A. Gangloff, G. Éthier-Majcher, C. Lang, E. V. Denning, J. H. Bodey, D. M. Jackson, E. Clarke, M. Hugues, C. Le Gall, and M. Atatüre, Quantum interface of an electron and a nuclear ensemble, Science **364**, 62 (2019).

[35] D. M. Jackson, U. Haeusler, L. Zaporski, J. H. Bodey, N. Shofer, E. Clarke, M. Hugues, M. Atatüre, C. Le Gall, and D. A. Gangloff, Optimal Purification of a Spin Ensemble by Quantum-Algorithmic Feedback, Phys. Rev. X **12**, 031014 (2022).

[36] C.-W. Huang and X. Hu, Theoretical study of nuclear spin polarization and depolarization in self-assembled quantum dots, Phys. Rev. B **81**, 205304 (2010).

[37] A. Högele, M. Kroner, C. Latta, M. Claassen, I. Carusotto, C. Bulutay, and A. Imamoglu, Dynamic nuclear spin polarization in the resonant laser excitation of an InGaAs quantum dot, Phys. Rev. Lett. **108**, 197403 (2012).

[38] L. Zhai, M. C. Löbl, G. N. Nguyen, J. Ritzmann, A. Javadi, C. Spinnler, A. D. Wieck, A. Ludwig, and R. J. Warburton, Low-noise GaAs quantum dots for quantum photonics, Nat. Commun. **11**, 4745 (2020).

[39] L. Zhai, G. N. Nguyen, C. Spinnler, J. Ritzmann, M. C. Löbl, A. D. Wieck, A. Ludwig, A. Javadi, and R. J. Warburton, Quantum interference of identical photons from remote GaAs quantum dots, Nat. Nanotechnol. **17**, 829 (2022).

[40] M. Reindl, D. Huber, C. Schimpf, S. F. C. da Silva, M. B. Rota, H. Huang, V. Zwiller, K. D. Jöns, A. Rastelli, and R. Trotta, All-photonic quantum teleportation using on-demand solid-state quantum emitters, Sci. Adv. **4**, eaau1255 (2018).

[41] E. A. Chekhovich, S. F. C. da Silva, and A. Rastelli, Nuclear spin quantum register in an optically active semiconductor quantum dot, Nat. Nanotechnol. **15**, 999 (2020).

[42] L. Zaporski, N. Shofer, J. H. Bodey, S. Manna, G. Gillard, M. H. Appel, C. Schimpf, S. F. Covre da Silva, J. Jarman, G. Delamare, G. Park, U. Haeusler, E. A. Chekhovich, A. Rastelli, D. A. Gangloff, M. Atatüre, and C. Le Gall, Ideal refocusing of an optically active spin qubit under strong hyperfine interactions, Nat. Nanotechnol. **18**, 257 (2023).

[43] See Supplemental Material at http://link.aps.org/supplemental/10.1103/PhysRevLett.131.210805 for methods of experiment, details on cooling parameters, and data analysis which includes Refs. [44–54].

[44] A. V. Kuhlmann, J. Houel, D. Brunner, A. Ludwig, D. Reuter, A. D. Wieck, and R. J. Warburton, A dark-field microscope for background-free detection of resonance fluorescence from single semiconductor quantum dots operating in a set-and-forget mode, Rev. Sci. Instrum. **84**, 073905 (2013).

[45] H. G. Babin, J. Ritzmann, N. Bart, M. Schmidt, T. Kruck, L. Zhai, M. C. Löbl, G. N. Nguyen, C. Spinnler, L. Ranasinghe, R. J. Warburton, C. Heyn, A. D. Wieck, and

A. Ludwig, Charge tunable GaAs quantum dots in a photonic n-i-p diode , Nanomaterials **11**, 2703 (2021).
[46] T. D. Ladd, D. Press, K. De Greve, P. L. McMahon, B. Friess, C. Schneider, M. Kamp, S. Höfling, A. Forchel, and Y. Yamamoto, Pulsed nuclear pumping and spin diffusion in a single charged quantum dot, Phys. Rev. Lett. **105**, 107401 (2010).
[47] R. Stockill, C. Le Gall, C. Matthiesen, L. Huthmacher, E. Clarke, M. Hugues, and M. Atatüre, Quantum dot spin coherence governed by a strained nuclear environment, Nat. Commun. **7**, 12745 (2016).
[48] M. C. Löbl, I. Söllner, A. Javadi, T. Pregnolato, R. Schott, L. Midolo, A. V. Kuhlmann, S. Stobbe, A. D. Wieck, P. Lodahl, A. Ludwig, and R. J. Warburton, Narrow optical linewidths and spin pumping on charge-tunable close-to-surface self-assembled quantum dots in an ultrathin diode, Phys. Rev. B **96**, 165440 (2017).
[49] P. Millington-Hotze, S. Manna, S. F. Covre da Silva, A. Rastelli, and E. A. Chekhovich, Nuclear spin diffusion in the central spin system of a GaAs/AlGaAs quantum dot, Nat. Commun. **14**, 2677 (2023).
[50] G. Wüst, M. Munsch, F. Maier, A. V. Kuhlmann, A. Ludwig, A. D. Wieck, D. Loss, M. Poggio, and R. J. Warburton, Role of the electron spin in determining the coherence of the nuclear spins in a quantum dot, Nat. Nanotechnol. **11**, 885 (2016).
[51] D. M. Jackson, D. A. Gangloff, J. H. Bodey, L. Zaporski, C. Bachorz, E. Clarke, M. Hugues, C. Le Gall, and M. Atatüre, Quantum sensing of a coherent single spin excitation in a nuclear ensemble, Nat. Phys. **17**, 585 (2021).
[52] P. Stano and D. Loss, Review of performance metrics of spin qubits in gated semiconducting nanostructures, Nat. Rev. Phys. **4**, 672 (2022).
[53] J. Yoneda, T. Otsuka, T. Nakajima, T. Takakura, T. Obata, M. Pioro-Ladrière, H. Lu, C. J. Palmstrøm, A. C. Gossard, and S. Tarucha, Fast electrical control of single electron spins in quantum dots with vanishing influence from nuclear spins, Phys. Rev. Lett. **113**, 267601 (2014).
[54] J. Medford, Ł. Cywiński, C. Barthel, C. M. Marcus, M. P. Hanson, and A. C. Gossard, Scaling of dynamical decoupling for spin qubits, Phys. Rev. Lett. **108**, 086802 (2012).
[55] J. H. Bodey, R. Stockill, E. V. Denning, D. A. Gangloff, G. Éthier-Majcher, D. M. Jackson, E. Clarke, M. Hugues, C. Le Gall, and M. Atatüre, Optical spin locking of a solid-state qubit, npj Quantum Inf. **5**, 95 (2019).
[56] S. R. Hartmann and E. L. Hahn, Nuclear double resonance in the rotating frame, Phys. Rev. **128**, 2042 (1962).
[57] X. Xu, W. Yao, B. Sun, D. G. Steel, A. S. Bracker, D. Gammon, and L. J. Sham, Optically controlled locking of the nuclear field via coherent dark-state spectroscopy, Nature (London) **459**, 1105 (2009).
[58] C. Kloeffel, P. A. Dalgarno, B. Urbaszek, B. D. Gerardot, D. Brunner, P. M. Petroff, D. Loss, and R. J. Warburton, Controlling the interaction of electron and nuclear spins in a tunnel-coupled quantum dot, Phys. Rev. Lett. **106**, 046802 (2011).
[59] B. Urbaszek, X. Marie, T. Amand, O. Krebs, P. Voisin, P. Maletinsky, A. Högele, and A. Imamoglu, Nuclear spin physics in quantum dots: An optical investigation, Rev. Mod. Phys. **85**, 79 (2013).
[60] I. T. Vink, K. C. Nowack, F. H. L. Koppens, J. Danon, Y. V. Nazarov, and L. M. K. Vandersypen, Locking electron spins into magnetic resonance by electron–nuclear feedback, Nat. Phys. **5**, 764 (2009).
[61] C. Latta, A. Högele, Y. Zhao, A. N. Vamivakas, P. Maletinsky, M. Kroner, J. Dreiser, I. Carusotto, A. Badolato, D. Schuh, W. Wegscheider, M. Atature, and A. Imamoglu, Confluence of resonant laser excitation and bidirectional quantum-dot nuclear-spin polarization, Nat. Phys. **5**, 758 (2009).
[62] F. K. Malinowski, F. Martins, Ł. Cywiński, M. S. Rudner, P. D. Nissen, S. Fallahi, G. C. Gardner, M. J. Manfra, C. M. Marcus, and F. Kuemmeth, Spectrum of the nuclear environment for GaAs spin qubits, Phys. Rev. Lett. **118**, 177702 (2017).
[63] L. Zaporski, S. R. de Wit, T. Isogawa, M. H. Appel, C. Le Gall, M. Atatüre, and D. A. Gangloff, A many-body singlet prepared by a central spin qubit, arXiv:2301.10258.